

# Direction-Dependent Power Curve Modeling for Multiple Interacting Wind Turbines

Mingdi You, *Student Member, IEEE*, Bingjie Liu, Eunshin Byon<sup>1</sup>, *Member, IEEE*, Shuai Huang, *Member, IEEE*, and Jionghua (Judy) Jin, *Member, IEEE*

**Abstract**—In industrial-scale wind farms, interactions among multiple turbines alter the power generation efficiency of turbines. In general, turbines in downwind rows are impacted by wind deficits, producing less power, compared to upstream turbines. Therefore, the generation performance of multiple turbines differs from one another. Moreover, the power curve of each turbine becomes heterogeneous when changes in wind direction cause some upstream turbines to become downstream turbines. This study proposes an integrative methodology that quantifies the heterogeneous wake effects over a range of wind direction by utilizing the concept of canonical models and similarity functions. We model the direction-dependent multi-turbine power curves in a Bayesian hierarchical framework and validate the performance of the proposed approach with multiple real-world data sets from industrial-scale wind farms.

**Index Terms**—Bayesian hierarchical framework, random effects, spatial modeling, wake effects, wind energy.

## I. INTRODUCTION

A RECENT trend of wind energy projects is to develop and operate a large-scale wind farm with multiple turbines. When multiple turbines are located close together, the resulting wake effects cause downstream turbines to produce less power than upstream turbines because the upstream turbines extract some of the energy in the wind [1]. Although it is recommended to maintain a certain minimum spacing between turbines to alleviate the negative influence of wake effects on power loss, often it is not practical due to local geography and economic constraints such as transmission costs, etc. [2].

Typically, the performance of individual turbines is quantified by its power curve which plots the power output against wind speed. In the literature, the power curve modeling at multiple turbines has been done through two steps in general [3]. At the first step, given the free-flow wind condition, the wind condition

Manuscript received November 9, 2016; revised March 14, 2017 and June 14, 2017; accepted August 1, 2017. Date of publication August 9, 2017; date of current version February 16, 2018. This work was supported by the National Science Foundation under Grants CMMI-1362513 and CMMI-1536924. Paper no. TPWRS-01692-2016. (*Corresponding author: Eunshin Byon.*)

M. You, B. Liu, E. Byon, and J. Jin are with the Department of Industrial and Operations Engineering, University of Michigan, Ann Arbor, MI 48109 USA (e-mail: mingdyou@umich.edu; bingjiel@umich.edu; ebyon@umich.edu; jhjin@umich.edu).

S. Huang is with the Department of Industrial and Systems Engineering, University of Washington, Seattle, WA 98105 USA (e-mail: shuaih@uw.edu).

This paper has supplementary downloadable material available at <http://ieeexplore.ieee.org>.

Color versions of one or more of the figures in this paper are available online at <http://ieeexplore.ieee.org>.

Digital Object Identifier 10.1109/TPWRS.2017.2737529

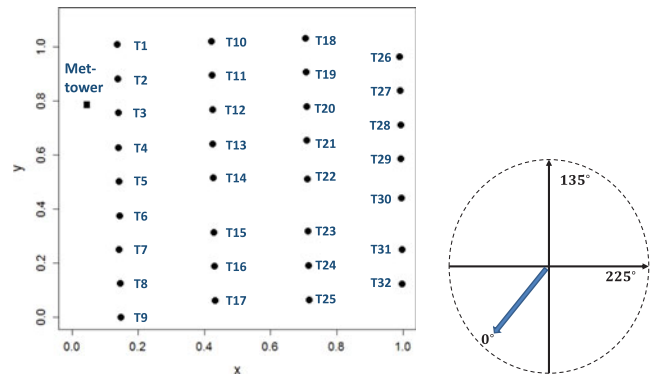


Fig. 1. Layout of WF1 (note: T<sub>n</sub> denotes the *n*th turbine.)

which each turbine faces is estimated. Existing studies in this step investigate how the wake interactions change the downstream speed, either using physics-based engineering models such as Jensen's model [4] or computational fluid dynamics (CFD) models that simulate the aerodynamics of wake effects to obtain the detailed wind profile [1]. At the second step, by plugging the estimated speed into the power curve, power output at each turbine is predicted. Recently, You *et al.* [5] propose a statistical approach that directly estimates the power generation level at each turbine, given the free-flow wind condition. Although their approach provides an insightful initial attempt to directly model the multi-turbine power curves, it is limited to a fixed wind direction. It still remains challenging to model heterogeneous power generation patterns over a range of wind directions.

This study provides an integrative framework that quantifies the power generation performance of multiple interacting turbines in all wind directions. To demonstrate the influence of wind directions on power generations in multiple turbines, we show the partial layout of a wind farm (referred to as WF1) in Fig. 1. For data confidentiality, we rotate and re-scale the layout and present a subset of turbines in the studied wind farm. In Fig. 1, dots correspond to turbine locations and the square represents the meteorology tower (met-tower). When wind blows from left to right, turbines in the leftmost column, T1 through T9, are upstream turbines. When wind direction changes, the wake correlations change accordingly and some of these turbines become downstream turbines.

To learn the heterogeneous power curves in different directions, we use a set of representative models, referred to as canon-

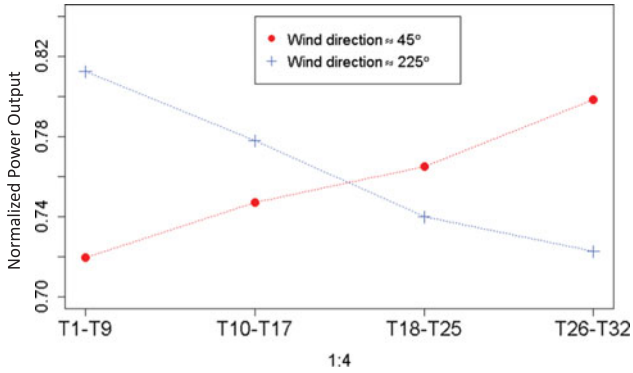


Fig. 2. Normalized average power generations under two different directions with the free-flow speed between 11.9 m/s and 12.1 m/s in WF1.

ical spatial models. Let us consider  $K$  canonical spatial models, each of which corresponds to its canonical wind direction. For example, with  $K = 4$ , we consider four spatial models representing the power variation patterns in four directions, e.g.,  $45^\circ$ ,  $135^\circ$ ,  $225^\circ$  and  $315^\circ$ . In practice, wind directions range between  $0^\circ$  and  $360^\circ$ . For example, when wind direction is  $70^\circ$ , the wake pattern would be similar to that in  $90^\circ$ , but also resemble the wake pattern in  $0^\circ$  to some extent. As such, in constructing power curves, we consider the similarities to the canonical models. We treat the canonical models as latent and integratively learn them by modeling the direction-dependent power curves in the Bayesian hierarchical inference and estimating the model parameters using the Markov Chain Monte Carlo (MCMC) [6].

The remainder of the paper is organized as follows. Section II describes the direction-dependent wake patterns. Section III discusses the proposed modeling and analysis procedure. Section IV presents a case study for evaluating the proposed model. Section V compares the proposed approach with alternative models. We summarize the paper in Section VI.

## II. DIRECTION-DEPENDENT POWER GENERATION PATTERNS

Fig. 2 shows the average power generations of the multiple turbines in WF1 under two different directions when the free-flow wind speed is between 11.9 and 12.1 meter per second (m/s). We normalize the power generation level in 0-1 (MW) scale. Each circle and ‘+’ represent the average power from turbines whose indexes are shown in the x-axis. As wind flows through turbines, the power outputs decrease. Specifically, the turbines in the rightmost column, T26 through T32, generate the least amount of power when the direction is  $225^\circ$ . We observe the opposite pattern under  $45^\circ$ .

Fig. 3 shows the power outputs from T8 and T32, where the x-axis and y-axis are the 10-minute average wind speed and normalized 10-minute average power output, respectively. In general, turbines generate more power as the wind speed increases from the cut-in speed of 4 m/s to the rated speed of about 15 m/s in WF1. Above the rated speed, their generation levels become steady due to the control algorithm to regulate power generation at high wind speeds. Despite the common trend exhibited by the two turbines, T8 tends to output less

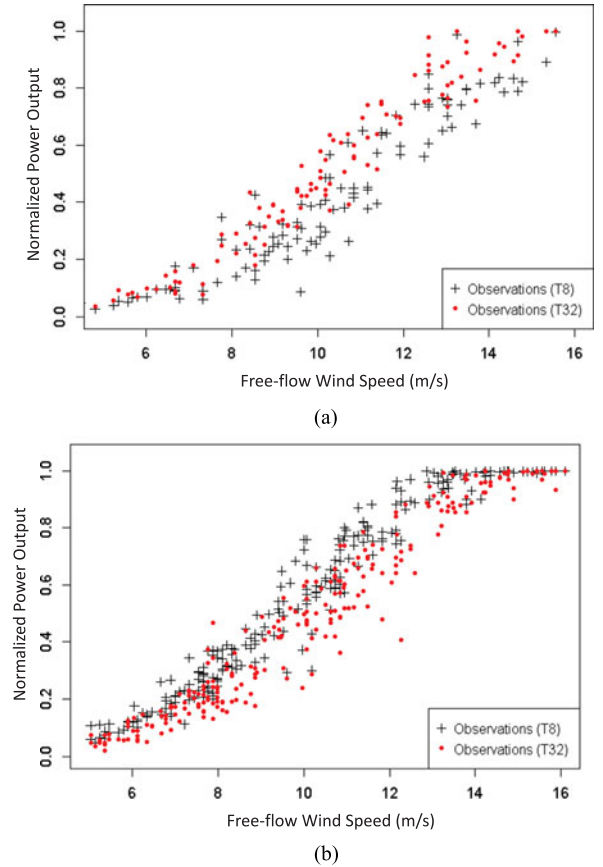


Fig. 3. Heterogeneous power generation patterns of T8 and T32 under two different wind directions in WF1. (a) When the wind direction is between  $40^\circ$  and  $50^\circ$ . (b) When the wind direction is between  $220^\circ$  and  $230^\circ$ .

power when wind direction is between  $40^\circ$  and  $50^\circ$  (Fig. 3(a)), but this pattern changes under  $220^\circ \sim 230^\circ$  (Fig. 3(b)). As a result, the power curves for individual turbines should differ, depending on the wind direction.

## III. METHODOLOGY

### A. Modeling Multi-Turbine Power Curves Under Wake Effects

We use data obtained from a real wind farm’s supervisory control and data acquisition (SCADA) system [7]. In a typical wind farm, the SCADA system collects 10-minute average data. Let  $P_{n,i}$  denote the 10-minute average power generation output of the  $n$ th turbine ( $n = 1, 2, \dots, N$ ) at the  $i$ th sample ( $i = 1, 2, \dots, I$ ) in the data set, where  $i$  denotes the time index at which the data sample is collected.

As seen in Fig. 3, turbines exhibit similar patterns, regardless of wind directions. We refer to such a common pattern as a global pattern. Depending on the locations of turbines and wind directions, however, some turbines generate more (or less) power than that of the global pattern. We refer to such variations as spatial variations. Considering both the global pattern and spatial variations, we formulate the power curve at each turbine as

$$P_{n,i} = G(v_i; \beta) + S(v_i, d_i; \eta_n, \gamma) + \epsilon_{n,i}, \quad (1)$$

for  $n = 1, \dots, N$  and  $i = 1, \dots, I$ , where  $v_i$  and  $d_i$  denote the 10-minute average free-flow wind speed and direction at the  $i$ th sample, respectively. It should be noted that the same free-flow wind speed  $v_i$  is used as an input covariate for all turbines. Components  $G(\cdot)$  and  $S(\cdot)$  represent the global pattern and spatial variations, respectively, with  $\beta$  and  $\gamma$  denoting the regression parameters, and  $\eta_n$  denoting a turbine-specific random effect which captures the turbine-to-turbine variations [5]. Parameters  $\beta$ ,  $\gamma$  and  $\eta_n$  need to be learned from the data (the specific meaning of these parameters and their estimation procedure will be detailed in subsequent discussions). The white noise  $\epsilon_{n,i}$  is assumed to be an independent Gaussian random variable with the mean 0 and variance  $\sigma^2$ .

The global pattern characterizes the general relationship between the power and wind speed. Therefore,  $G(v_i; \beta)$  in (1) does not include the direction  $d_i$  and turbine index  $n$ , and the same  $\beta$  is shared by all turbines under all directions. We model  $G(v_i; \beta)$  with a regression function as

$$G(v_i; \beta) = V_{g,i} \beta, \quad (2)$$

where  $V_{g,i}$  is a row vector in the design matrix corresponding to  $v_i$ , and  $\beta$  is a column vector consisting of associated regression coefficients. For example, if we use a quadratic function between cut-in and rated speeds,  $V_{g,i}$  becomes  $[1, v_i, v_i^2]$  and  $V_{g,i} \beta$  takes a form of  $V_{g,i} \beta = \beta_0 + \beta_1 v_i + \beta_2 v_i^2$  with the parameter vector  $\beta = [\beta_0, \beta_1, \beta_2]^T$ . For the speed between the rated and cut-out speeds, a constant function can be used. More flexible functions, e.g., splines, can be used to capture the non-linear pattern in the power curve [8], [9].

In contrast to the global trend shared by all turbines, the term  $S(v_i, d_i; \eta_n, \gamma)$  in (1) is turbine-dependent with the turbine-specific parameter  $\eta_n$ , and it captures the influence of wake interactions among turbines on power generations. The spatial variations should also depend on the wind direction  $d_i$ . To characterize the heterogeneous spatial variations over a range of wind directions, we propose to use a set of canonical spatial models. We first present our approach for building canonical models and then generalize the canonical models to capture the wake interactions in any wind directions.

Let us consider  $K$  canonical spatial models. The number  $K$  can be pre-specified using domain knowledge or learned from data (in Section IV we discuss the effect of  $K$  on the estimation accuracy). Let  $c_1, c_2, \dots, c_K$  denote  $K$  pre-specified canonical wind directions. The  $k$ th canonical model  $S(v_i, c_k; \eta_{nk}, \gamma_k)$  represents the spatial variation of the  $n$ th turbine's output, i.e., the discrepancy between the output from the  $n$ th turbine and the output in the global term when the wind direction and speed are  $c_k$  and  $v_i$ , respectively. To represent the canonical model  $S(v_i, c_k; \eta_{nk}, \gamma_k)$ , we use a modeling approach similar to the global model in (2). Unlike the global model, however, this spatial term should address the turbine-to-turbine variations, i.e.,  $S(v_i, c_k; \eta_{nk}, \gamma_k)$  at each turbine should differ. Therefore, we introduce the random effect  $\eta_{nk}$  as proposed in [5] and model the  $k$ th canonical model as

$$S(v_i, c_k; \eta_{nk}, \gamma_k) = \eta_{nk} V_{s,i} \gamma_k, \quad k = 1, 2, \dots, K. \quad (3)$$

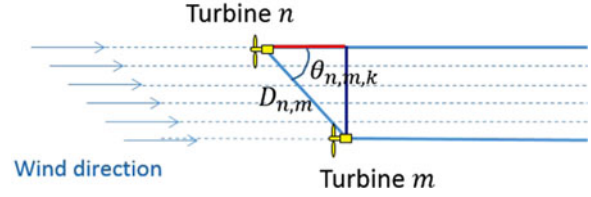


Fig. 4. Direction-dependent intensity between two turbines.

Here, noting that the power deficit is heterogeneous over a range of wind speeds even under the same wind direction, we formulate  $S(v_i, c_k; \eta_{nk}, \gamma_k)$  as a function of wind speed with a row vector  $V_{s,i}$  in the design matrix and the corresponding regression parameter vector  $\gamma_k$ .

The turbine-specific parameter  $\eta_{nk}$  in (3) captures the wake interactions among turbines, and thus,  $\eta_{nk}$  should depend on neighbor turbines. We formulate  $\eta_{nk}$  with the Gaussian Markov random field (GMRF) [6] as

$$\eta_{nk} | \{\eta_{mk} : m \in \mathcal{N}(n)\} \sim N \left( \sum_{m \in \mathcal{N}(n)} z_{n,m,k} \eta_{mk}, \tau_k^2 \right), \quad (4)$$

for  $n, m = 1, 2, \dots, N (n \neq m)$ , and  $k = 1, 2, \dots, K$ , where  $\mathcal{N}(n)$  is the set of turbine  $n$ 's neighbor turbines and  $\tau_k^2$  is the conditional variance of  $\eta_{nk}$ . We define  $\mathcal{N}(n)$  as the set of turbine  $n$ 's surrounding turbines. Parameter  $z_{n,m,k}$  is the dependence intensity between turbine  $n$  and its neighboring turbine  $m$ . For the two turbines placed close to each other, the dependence intensity  $z_{n,m,k}$  should be large. We model  $z_{n,m,k}$  using a direction-dependent intensity model that considers both distance and direction [10]:

$$z_{n,m,k} = \delta_{1,k} \sin^2(\theta_{n,m,k}) D_{n,m}^{-h} + \delta_{2,k} \cos^2(\theta_{n,m,k}) D_{n,m}^{-h}, \quad (5)$$

where  $D_{n,m}$  is the distance between turbines  $n$  and  $m$ , and  $\theta_{n,m,k}$  is the angle between two turbines under  $c_k$ . Parameters  $\delta_{1,k}$  and  $\delta_{2,k}$  measure the dependence intensity in the orthogonal of and parallel to the wind direction, respectively (Fig. 4). Scalar  $h$  ( $h > 0$ ) is the scaling parameter that represents how quickly the intensity diminishes as the distance becomes larger.

Because the canonical spatial models capture the spatial variations under specific wind directions only, we need to generalize the canonical models in order to characterize the spatial variations under any directions. Clearly, when wind direction  $d_i$  is close to canonical wind direction  $c_k$ , the wake interaction patterns under direction  $d_i$  should be similar to that under direction  $c_k$ . The power generation pattern will also resemble the pattern under another adjacent canonical direction. Therefore, we model the spatial term  $S(v_i, d_i; \eta_n, \gamma)$  in (1) using the weighted combination of two adjacent canonical models. Let  $w_k(d_i)$  denote a similarity function between the  $k$ th canonical direction  $c_k$  and the direction  $d_i$  in the  $i$ th sample. We formulate  $S(v_i, d_i; \eta_n, \gamma)$  as

$$S(v_i, d_i; \eta_n, \gamma) = \sum_{k=1}^K w_k(d_i) S(v_i, c_k; \eta_{nk}, \gamma_k), \quad (6)$$

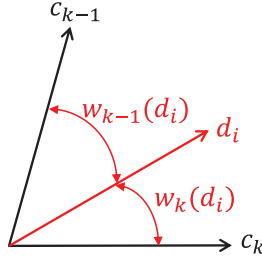


Fig. 5. Canonical wind directions and similarity functions.

for  $i = 1, \dots, I$ , where  $w_k(d_i)$  is non-zero when  $c_k$  is one of the two adjacent directions of  $d_i$  and zero for other non-adjacent directions (Fig. 5).

We define  $w_k(d_i)$  with the Gaussian kernel [11] as

$$w_k(d_i) \propto \begin{cases} \exp\left(-\frac{\|d_i - c_k\|^2}{\psi}\right), & \text{if } d_i \text{ is adjacent to } c_k; \\ 0, & \text{otherwise} \end{cases} \quad (7)$$

Here,  $\|d_i - c_k\|$  is defined as  $\min\{|d_i - c_k|, |360^\circ - (d_i - c_k)|\}$ . For example, for  $d_i = 350^\circ$  and  $c_1 = 90^\circ$ , the difference between the two directions should be  $100^\circ$  instead of  $260^\circ$ . Note that  $w_k(d_i)$  assigns a higher similarity measure to the direction that has a smaller difference. Scalar  $\psi$  quantifies how quickly the similarity decreases when  $d_i$  differs from  $c_k$ . We normalize  $w_k(d_i)$  such that the sum of two non-zero weights becomes 1, i.e.,  $\sum_{k=1}^K w_k(d_i) = 1$ , for each data sample  $i$ .

## B. Parameter Estimation

To learn the canonical models and model parameters, we use the Bayesian hierarchical framework with three levels. The first level, which we refer to as the data model, specifies the model for the power output, given the canonical model and model parameters. With the global pattern in (2) and spatial variations in (6), the power output becomes

$$P_{n,i} = V_{g,i}\beta + \sum_{k=1}^K w_k(d_i)\eta_{nk}V_{s,i}\gamma_k + \epsilon_{n,i}, \quad (8)$$

and its likelihood function is

$$\begin{aligned} f(P_{n,i} | V_{g,i}, V_{s,i}, \beta, \eta, \gamma, \sigma) \\ = N\left(V_{g,i}\beta + \sum_{k=1}^K w_k(d_i)\eta_{nk}V_{s,i}\gamma_k, \sigma^2\right), \end{aligned} \quad (9)$$

for  $n = 1, 2, \dots, N, i = 1, \dots, I$ , where  $\eta$  and  $\gamma$  denote sets of  $\eta_k$ 's and  $\gamma_k$ 's ( $k = 1, \dots, K$ ), respectively.

The second level specifies the spatial process model. With the conditional distribution for  $\eta_{nk}$  in (4), the joint distribution of  $\eta_k = [\eta_{1k}, \eta_{2k}, \dots, \eta_{Nk}]^T$  for each  $k$  becomes the multivariate normal distribution [6],

$$p(\eta_k | \delta_{1,k}, \delta_{2,k}, \tau_k^2) = MVN(0, \tau_k^2(\mathbb{1} - Z_k)), \quad (10)$$

where  $\mathbb{1}$  is the identity matrix and  $Z_k$  is an  $N \times N$  matrix whose  $(n, m)$ th off-diagonal element is  $z_{n,m,k}$  in (5) and all diagonal elements are zeros.

The third level specifies a prior density for each parameter. Let  $\theta$  denote a set of model parameters,  $\beta, \gamma_k, \sigma^2, \tau_k^2, \delta_{1,k}, \delta_{2,k}$  ( $k = 1, \dots, K$ ). Then the parameter model is

$$p(\theta) \sim \text{prior}(\theta). \quad (11)$$

In (11), we use conjugate priors for  $\beta, \gamma_k, \tau_k^2$ , and  $\sigma^2$ . Specifically, we use the multivariate normal distribution for  $\beta$  and  $\gamma_k$  and the inverse Gamma distribution for  $\tau_k^2$  and  $\sigma^2$  [6]. For  $\delta_{1,k}$  and  $\delta_{2,k}$ , there are no conjugate priors, so we use uniform distributions to impose non-informative priors.

With the Bayesian hierarchical formulation, we obtain the joint posterior distribution of  $\eta_k$ 's and  $\theta$  as

$$p(\eta_1, \eta_2, \dots, \eta_K, \theta) \propto$$

$$\prod_{n,i} \prod_k f(P_{n,i} | V_{g,i}, V_{s,i}, \beta, \eta_k, \gamma_k, \sigma) p(\eta_k | \delta_{1,k}, \delta_{2,k}, \tau_k^2) p(\theta). \quad (12)$$

Because the joint posterior in (12) does not take a closed form, we use a sampling-based MCMC approach to simulate posterior samples for the model parameters. We implement MCMC using the WinBUGS software by calling WinBUGS [12] from the R package [13]. Under the Bayesian hierarchical framework, all of the model parameters, except  $\delta_{1,k}$  and  $\delta_{2,k}$ , have the closed-form full conditionals (see the online supporting document). Therefore, their posterior samples are drawn using Gibbs sampling. For  $\delta_{1,k}$  and  $\delta_{2,k}$ , we note that their full conditional densities are log-concave, and WinBUGS employs the adaptive rejection sampling when the full conditionals are log-concave [12], [14]. Given the posterior samples, we use posterior means for estimating  $\beta, \gamma_k$  and  $\eta_{nk}$ , denoted as  $\hat{\beta}, \hat{\gamma}_k$  and  $\hat{\eta}_{nk}$ , respectively, and estimate the direction-dependent power curve of each turbine as

$$\hat{P}_{n,i} = V_{g,i}\hat{\beta} + \sum_{k=1}^K w_k(d_i)\hat{\eta}_{nk}V_{s,i}\hat{\gamma}_k, \quad (13)$$

for  $n = 1, 2, \dots, N, i = 1, \dots, I$ .

## C. Learning Latent Canonical Models

This section provides insights into how the proposed canonical models, which are latent and learned from the data, integratively represent the wake correlations over a range of wind directions. In the Gibbs sampling procedure, the posterior sample for  $\eta_k$  is obtained from  $MVN(\mu_{\eta_k}, Q_{\eta_k}^{-1})$  with

$$\begin{aligned} \mu_{\eta_k} &= \frac{1}{\sigma^2} Q_{\eta_k}^{-1} \\ &\times \left[ \sum_{i=1}^I w_k(d_i) \gamma_k^T V_{s,i}^T (P_i - V_{g,i} \beta) \mathbb{1}_{N \times 1} - \sum_{j \neq k} w_j(d_i) V_{s,i} \gamma_j \eta_j \right], \end{aligned} \quad (14)$$

$$Q_{\eta_k} = \frac{1}{\tau_k^2} (\mathbb{1} - Z_k)^{-1} + \sum_{i=1}^I \frac{1}{\sigma^2} (w_k(d_i) V_{s,i} \gamma_k)^2 \mathbb{1}, \quad (15)$$

where  $P_i = [P_{1,i}, P_{2,i}, \dots, P_{N,i}]^T$  and  $\mathbb{1}_{N \times 1}$  is a vector with all elements being 1 (see the online supporting document for details).

These density parameters in (14) and (15) provide several important insights. First, the density parameters, which depend on  $w_k(d_i)$ , show that how the  $i$ th sample obtained under the direction  $d_i$  affects the posterior density of  $\eta_k$  (Fig. 5). Each data sample has a different role in learning each canonical model through the similarity function  $w_k(d_i)$ . The data sample with a higher  $w_k(d_i)$ , i.e., when  $d_i$  is close to  $c_k$ , will have a greater impact on  $\eta_k$ 's density parameters  $\mu_{\eta_k}$  and  $Q_{\eta_k}$ . Second, the last term  $\sum_{j \neq k}^K w_j(d_i) V_{s,i} \gamma_j \eta_j$  inside the parentheses in (14), indicates that  $\eta_k$  is correlated with other  $\eta_j$ 's. Therefore, all canonical models are correlated with one another, implying that all of the data samples are collectively used for learning multiple canonical models. Moreover, the full conditional of  $\eta_k$  in (14) and (15) differs from the prior density in (4). The density in (4) formulates the *prior* correlation structure with our initial knowledge on the turbine-to-turbine interactions without using any information from the data. Under the Bayesian hierarchical modeling framework, we estimate  $\eta_k$  using the joint information of the prior and observed data. The posterior density of  $\eta_k$  provides such insights in the Bayesian inference.

#### IV. CASE STUDY

We use 1000 samples from WF1 and implement MCMC with WinBUGS [12] and R [13] packages.

##### A. Implementation Details

In our model in (1),  $v_i$  represents the free-flow wind speed at the  $i$ th data sample. Typical wind farms have one (or a few) met-towers collecting free flow wind speeds in dominant wind directions. Our single met-tower provides free-flow wind conditions when the wind blows from west to east (Fig. 1). When it blows in different directions, the wind flow passing the met-tower is heavily disturbed by other turbines, and as a result, data collected from the met-tower does not represent the free-flow wind condition. To obtain the free-flow wind speed in any wind direction, we use the Nacelle Transfer Function (NTF), which uses the wind speed collected at the turbine anemometer and the speed measured at the met-tower [15]. For the detailed procedure of NTF, we refer readers to [15].

For small-scale wind farms that do not have a met-tower, other approaches should be employed to obtain the free-flow wind speed. Additionally, we would like to point out that with a limited number of neighbor turbines in a small-scale wind farm, the advantage of our approach would be limited. This is because our approach utilizes data from neighbor turbines for characterizing the spatial correlations among turbines. As such, our approach would be useful for industrial-scale wind farms with dozens or hundreds of turbines.

For the global pattern in (2) and canonical models in (3), we use the B-spline because of its flexible modeling capability [11]. We decide the degree of spline and the internal knots empirically. After extensive preliminary analysis, we use the B-spline of degree 2 with five internal knots at 5 m/s, 7.5 m/s, 10 m/s, 12.5 m/s, and 15 m/s for both global and spatial terms. For  $h$  in (5), we use 0.5. For  $\psi$  in (7), our analysis with a wide range from 1 to 100 suggests that the performance of the

TABLE I  
AVERAGE RMSE AND MAE FROM 10-FOLD CV WITH DIFFERENT NUMBERS OF CANONICAL MODELS IN WF1 (UNIT: NORMALIZED POWER IN [0, 1] MW)

$K$	RMSE	MAE
4	0.069	0.047
6	0.067	0.047
8	0.066	0.046
12	0.067	0.046

proposed approach is not sensitive to the choice of  $\psi$ . In our analysis, we use  $\psi = 20$ .

In implementing MCMC, we discard the results from the first 5000 iterations as a burn-in period to wait until the Markov chain becomes fully stationary. We use the next 5000 samples to closely approximate the posterior distribution. Determining the burn-in period and number of posterior samples is beyond the scope of this study, so we refer interested readers to [16]. Partial results of parameter estimates and trace plots are available in the online supporting document.

##### B. Implementation Results

We implement the proposed approach with different numbers of canonical models. For each case, we consider evenly spaced canonical directions. For example, with  $K = 8$ , we set  $c_1 = 22.5^\circ, c_2 = 67.5^\circ, c_3 = 112.5^\circ, \dots, c_8 = 337.5^\circ$  (in Section IV-C, we consider another choice of canonical directions to investigate the robustness of our approach). To evaluate the performance, we employ ten-fold cross validation (CV), i.e., we randomly divide the entire data set into 10 sets, and train the model with 9 sets, and test the estimation performance with the remaining set. We repeat this procedure 10 times with 10 different test sets. In the 10-fold CV, each training set includes data over the full range of wind directions. The accuracy of proposed approach is measured with root mean square error (RMSE) and mean absolute error (MAE).

Table I lists the estimation results of the proposed approach with different numbers of canonical models. It is interesting to see that the results are not sensitive to different canonical models. The RMSE and MAE of each model are within 1 standard deviation of other models in the 10-fold CV. This indicates that the similarity function defined in (7) can successfully capture the wake correlations between the canonical directions, even when a small number of canonical models are employed. The result with  $K = 8$  provides the best results, and we use it in the remaining analysis.

Fig. 6(a) shows the estimated power curves of T8 and T32 under wind direction  $45^\circ$  and actual observations collected under  $40^\circ \sim 50^\circ$ . T8 generates less power than T32, as it is the downstream under  $45^\circ$ . In Fig. 6(b), the estimated power curves of T8 and T32 under  $225^\circ$  can be explained likewise. Fig. 7 depicts that T18 generates larger power outputs under  $315^\circ$  compared to those under other two directions.

Fig. 8(a) shows the estimated power generation of T8 under  $[0^\circ, 360^\circ]$  when wind speed is 12 m/s. The radius is the estimated power under the corresponding direction. T8 generates

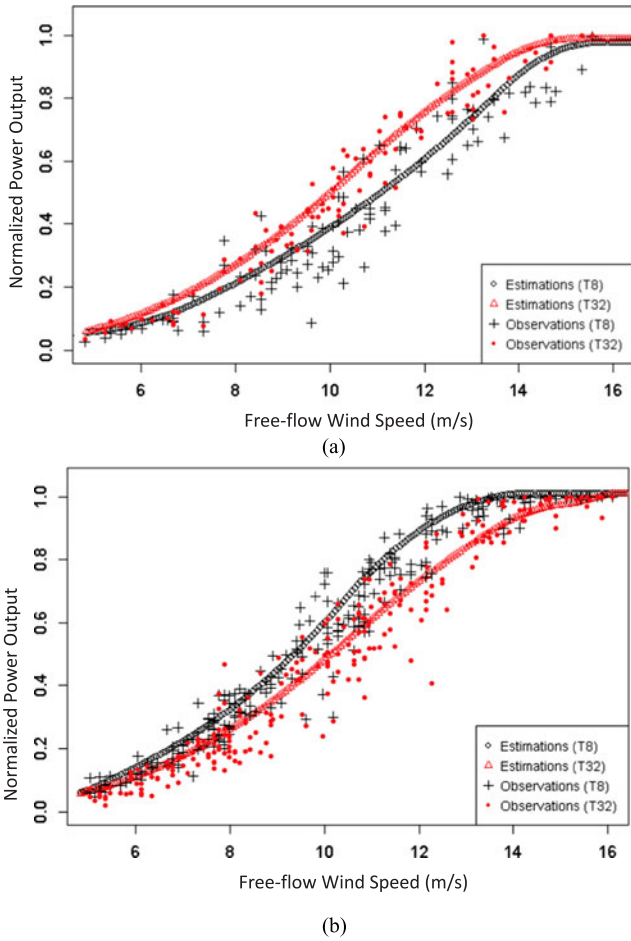


Fig. 6. Estimated and observed power outputs of T8 and T32 in WF1. (a) Estimated power curves under  $45^\circ$  and actual observations under  $40^\circ \sim 50^\circ$ . (b) Estimated power curves under  $225^\circ$  and actual observations under  $220^\circ \sim 230^\circ$ .

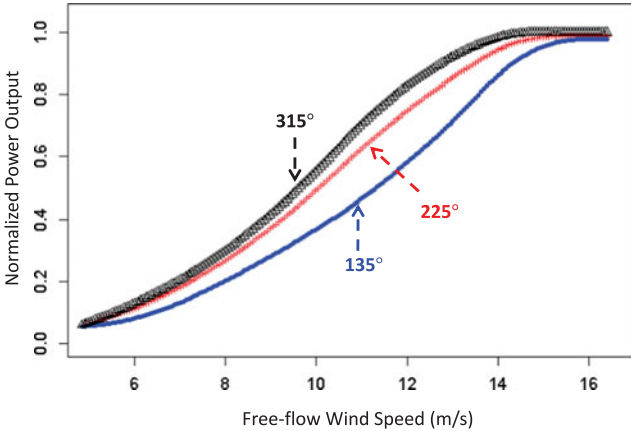


Fig. 7. Estimated power curve of T18 under different directions in WF1.

more power when wind direction ranges over  $180^\circ \sim 270^\circ$  as it is the upstream turbine under this range, whereas it generates less power under  $315^\circ \sim 90^\circ$ . On the contrary, Fig. 8(b) demonstrates that the power generation of T21 is not sensitive to the direction because it is located inside the wind farm.

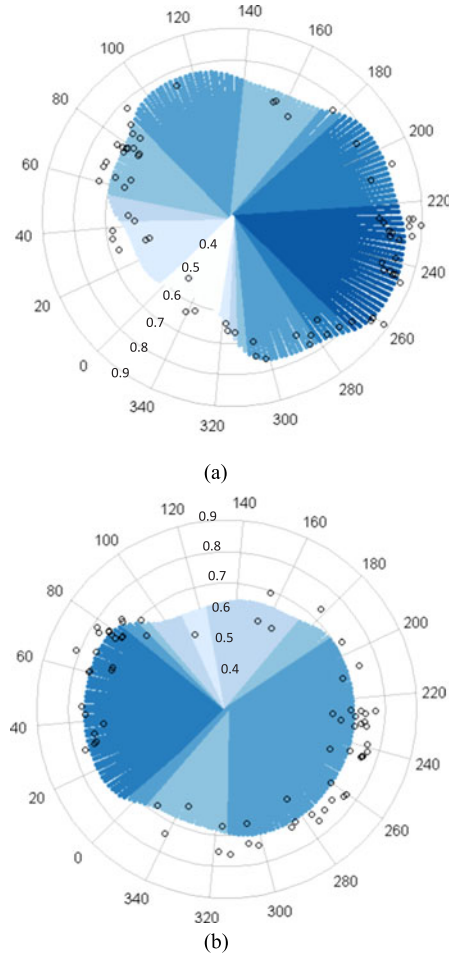


Fig. 8. Estimated power when wind speed is 12 m/s in WF1 (Note: The small circles denote the observed power outputs at 11.9 m/s  $\sim$  12.1 m/s). (a) T8. (b) T21.

### C. Sensitivity Analysis on Canonical Wind Directions

To investigate the effect of the locations of canonical directions, we also implement the proposed approach with a different choice of canonical directions. Specifically, noting that in general, wind directions are not evenly distributed over  $[0^\circ, 360^\circ]$ , we consider the distribution of wind directions at the wind farm site. We decompose the direction such that each sector  $[c_{k-1}, c_k]$ ,  $k = 1, \dots, K$ , includes the same number of samples with  $K = 8$ . Therefore, under the high frequency direction range (i.e., dominant wind directions), the sector between two canonical directions is narrow, whereas the sector is wide under the low frequency direction range. The resulting average RMSE and MAE from the 10-fold CV with this set of unevenly spaced canonical directions are 0.066 and 0.046, respectively, which are very close to the estimation errors in Table I. This result suggests the robustness of the proposed approach on the choice of canonical directions.

### V. COMPARISON WITH ALTERNATIVE APPROACHES

We compare the performance of the proposed approach with several alternatives. In addition to WF1, we use additional data

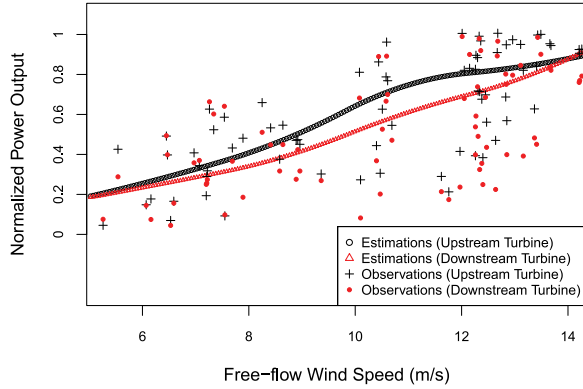


Fig. 9. Estimated and observed power outputs from a pair of turbines in WF2.

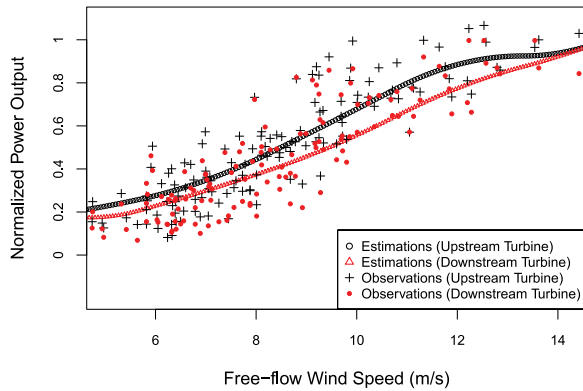


Fig. 10. Estimated and observed power outputs from a pair of turbines in WF3.

sets from two operating wind farms, called WF2 and WF3. Both WF2 and WF3 have about 40 turbines. We omit the detailed descriptions of the wind farms due to data confidentiality. Figs. 9 and 10 show the estimated and observed power outputs from a pair of turbines in WF2 and WF3, respectively.

The first alternative is Jensen's model, which is one of the most popular physics-based engineering models [4]. Jensen's model analytically estimates wind speeds at downstream turbines. We combine the wind speed estimates obtained from Jensen's model with the quadratic power curve between the cut-in and rated wind speed to estimate the power output [17]. We also implement the authors' prior work in [5] using data in the dominant direction and apply the resulting power curves to estimate the power outputs over all directions. This approach is called an approach with dominant direction.

Moreover we consider three individual models that have turbine-specific spline regression parameters:

$$(IND1) : P_{n,i} = V_i \beta_n + D_i \gamma_n + \epsilon_{n,i}, \quad (16)$$

$$(IND2) : P_{n,i} = V_i \beta_n + D_i \gamma_n + T_i \lambda_n + \epsilon_{n,i}, \quad (17)$$

$$(IND3) : P_{n,i} = V_{s,i} \beta_n + V_{c,i} \gamma_n + \epsilon_{n,i}, \quad (18)$$

for  $n = 1, \dots, N$  and  $i = 1, \dots, I$ . Here, in IND1,  $V_i$  and  $D_i$  are the row vectors in the design matrices corresponding to the wind speed  $v_i$  and direction  $d_i$ , respectively. We employ the B-spline

TABLE II  
PERFORMANCE COMPARISON (UNIT: NORMALIZED POWER IN [0, 1] MW)

(a) RMSE			
	WF1	WF2	WF3
Proposed approach	0.066	0.150	0.153
Jensen's model	0.085*	0.171*	0.179*
Approach with dominant direction [5]	0.086*	0.160*	0.160*
IND1	0.070	0.156*	0.157*
IND2	0.068	0.154*	0.161*
IND3	0.089*	0.169*	0.193*
(b) MAE			
	WF1	WF2	WF3
Proposed approach	0.046	0.119	0.118
Jensen's model	0.064*	0.135*	0.134*
Approach with dominant direction [5]	0.059*	0.128*	0.124*
IND1	0.049*	0.124*	0.121*
IND2	0.048*	0.122*	0.123*
IND3	0.063*	0.127*	0.135*

Note: The '\*' denotes that the p-value in the statistical testing to compare the difference between the proposed approach and each alternative is less than 5%. Since p-values are less than 5% in most cases, it indicates that the proposed approach is consistently better than all other methods.

for the wind speed and the cyclic B-spline for the wind direction. In IND2, we additionally include the interaction term  $T_i$  between wind speed and direction, where  $T_i$  is the row vector of the B-spline design matrix associated with the predictor  $v_i d_i$ . In IND3,  $V_{s,i}$  and  $V_{c,i}$  denote the row vectors of the B-spline design matrix corresponding to  $v_i \sin(d_i)$  and  $v_i \cos(d_i)$ , respectively. Note that all three individual models have turbine-specific parameters. In each model, the model parameters are estimated separately using the power output data from each turbine, resulting in  $N$  regression functions.

Table II compares the estimation performance of the proposed approach with alternative models from the 10-fold CV. The proposed approach generates the lowest prediction errors in all cases. To evaluate the significant difference between the proposed model and each alternative, we perform hypothesis tests using the statistical t-test. In most cases, the p-values are less than the commonly used significance level 5%, suggesting that the prediction errors from the proposed model are significantly smaller than those from other approaches.

In general, Jensen's model generates higher prediction errors, compared with other alternatives. The result of the approach with dominant direction indicates that the power curves fitted under a fixed direction are not adequate to estimate the power outputs under other directions. Among the alternative models, the individual modeling approach, in particular, IND1 or IND2, generally performs better than other models. However, its estimation capability appears to be worse than the proposed model. We summarize the advantages of our approach over individual approach.

- 1) Our approach takes a collaborative learning scheme to fit the power curves. To estimate the power curve of one turbine, data from other turbines is also utilized, so we can borrow the strength from the information obtained from other turbines.

- 2) Physical characteristics about the wake effects are explicitly reflected by the proposed method via the following aspects: (a) the GMRF modeling for the turbine-specific parameter  $\eta_{n,k}$  in (4) captures the spatial correlations among neighbor turbines; (b) the interaction intensity  $z_{n,m,k}$  in (5) incorporates the effect of both the distance between turbines and wind direction on the turbines' power generation patterns; and moreover (c) the similarity function  $w_k(d_i)$  in (7) accounts for the similar wake pattern in close wind directions, providing another layer of collaborative learning scheme.
- 3) The advantage of the proposed approach becomes more beneficial when the power curves are estimated with noisy observations. Compared to WF1, turbines' power outputs in WF2 and WF3 are much more noisy (see Figs. 9 and 10). Despite the large noise, the fitted power curves from our approach estimate the heterogeneous patterns successfully. We believe this is because our approach takes the collaborative learning scheme and accounts for the physical understanding about wake effects in the power curve estimations, as discussed above.

## VI. CONCLUDING REMARKS AND FUTURE PLANS

This study develops an integrative approach for fitting the direction-dependent power curves of multiple interacting wind turbines. Our approach uses a combination of canonical models and similarity functions to capture the wake correlations in any wind directions. A comprehensive case study suggests that the proposed approach improves the estimation accuracy of power outputs from the multiple turbines when compared with the widely employed Jensen's model and other individual approaches. The results also suggest that applying the power curves constructed under a specific direction is not adequate to achieve a high estimation accuracy in other directions.

Although we use only wind speed and direction to fit the power curves due to the available data in the studied data sets, the proposed model can be extended to include other environmental factors. For example, one possible way is to use geostrophic wind that accounts for the effects of air pressure and temperature [18]. Alternatively, we can include other environmental factors as additional covariates in our proposed model [19]. In terms of the learning method, instead of MCMC, the variational Bayes can be employed to reduce the computational time for estimating model parameters.

The proposed approach can provide a stepping stone to improve the performance of wind farm operations. In the literature, data-driven parametric models have been studied for optimizing the control to maximize the outputs from the wind farm. For example, Gebraad *et al.* [20] propose a model where the parameters are estimated using data and obtain the optimal yaw control set points that can maximize the total energy generation. However, their method focuses on estimating downstream speeds and is applied to a small wind farm at a certain wind speed. The spatial modeling method introduced in our paper provides an explicit parametric representation, which shows its capability of capturing the interactions among wind turbines

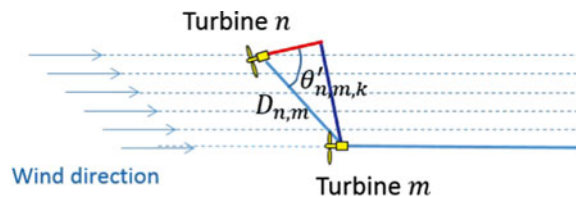


Fig. 11. Illustration of the change of interaction intensity due to yaw control.

under potential control settings. For example, in our model,  $z_{n,m,k}$  in (5) quantifies the interaction intensity as a parametric form of  $\theta_{n,m,k}$ . This function can be potentially extended to parameterize the correlations under different yaw control points. If a yaw control changes the direction  $\theta_{n,m,k}$  to  $\theta'_{n,m,k}$  (Fig. 11), the interaction intensity changes accordingly. This parametric form has a potential for finding the optimal control set points of multiple interacting turbines.

Our model can be also used as a surrogate model of sophisticated CFD model for the layout design optimization. The CFD model can achieve a high accuracy in estimating the wake effects, but with a greater computational cost. To overcome the computational difficulty, we can generate a small number of samples from the CFD model to build the proposed model. In particular, in our model, the correlation structure among multiple turbines depends on the distance among turbines as shown in (5). By generating samples in different distances, we can parameterize the correlation as a function of distance and optimize the inter-distances among turbines. Alternatively, our approach can be used to link the CFD model with Jensen's model. In the literature, surrogate models have been used to link multi-fidelity models [21], based on which the layout optimization can be performed.

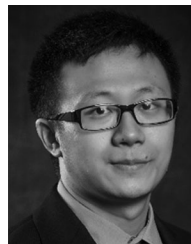
## REFERENCES

- [1] E. S. Politis, J. Prospathopoulos, D. Cabezon, K. S. Hansen, P. K. Chaviaropoulos, and R. J. Barthelmie, "Modeling wake effects in large wind farms in complex terrain: The problem, the methods and the issues," *Wind Energy*, vol. 15, no. 1, pp. 161–182, 2012.
- [2] S.-H. Kim, H.-K. Shin, Y.-C. Joo, and K.-H. Kim, "A study of the wake effects on the wind characteristics and fatigue loads for the turbines in a wind farm," *Renew. Energy*, vol. 74, pp. 536–543, 2015.
- [3] M. Khalid and A. V. Savkin, "A method for short-term wind power prediction with multiple observation points," *IEEE Trans. Power Syst.*, vol. 27, no. 2, pp. 579–586, May 2012.
- [4] N. O. Jensen, "A note on wind generator interaction," Riso Nat. Lab., Tech. Univ. Denmark, Roskilde, Denmark, Tech. Rep. Riso-M-2411, 1983.
- [5] M. You, E. Byon, J. Jin, and G. Lee, "When wind travels through turbines: A new statistical approach for characterizing heterogeneous wake effects in multi-turbine wind farms," *IJSE Trans.*, vol. 49, no. 1, pp. 84–95, 2017.
- [6] S. Banerjee, B. P. Carlin, and A. E. Gelfand, *Hierarchical Modeling and Analysis for Spatial Data*. Boca Raton, FL, USA: CRC Press, 2014.
- [7] N. Yampikulsakul, E. Byon, S. Huang, S. Shawn, and Y. Mingdi, "Condition monitoring of wind turbine system with nonparametric regression-based analysis," *IEEE Trans. Energy Convers.*, vol. 29, no. 2, pp. 288–299, Jun. 2014.
- [8] G. Lee, E. Byon, L. Ntamo, and Y. Ding, "Bayesian spline method for assessing extreme loads on wind turbines," *Ann. Appl. Statist.*, vol. 7, no. 4, pp. 2034–2061, 2013.
- [9] Y. Choe, E. Byon, and N. Chen, "Importance sampling for reliability evaluation with stochastic simulation models," *Technometrics*, vol. 57, no. 3, pp. 351–361, 2015.
- [10] M. S. Kaiser, M. J. Daniels, K. Furakawa, and P. Dixon, "Analysis of particulate matter air pollution using Markov random field models of spatial dependence," *Environmetrics*, vol. 13, no. 5/6, pp. 615–628, 2002.

- [11] J. Friedman, T. Hastie, and R. Tibshirani, *The Elements of Statistical Learning: Data Mining, Inference, and Prediction*. New York, NY, USA: Springer, 2009.
- [12] D. Lunn, C. Jackson, N. Best, A. Thomas, and D. Spiegelhalter, *The BUGS Book: A Practical Introduction to Bayesian Analysis*. Boca Raton, FL, USA: CRC Press, 2012.
- [13] S. Sturtz, U. Ligges, and A. E. Gelman, "R2WinBUGS: A package for running WinBUGS from R," *J. Statist. Softw.*, vol. 12, no. 3, pp. 1–16, 2005.
- [14] W. R. Gilks and P. Wild, "Adaptive rejection sampling for Gibbs sampling," *Appl. Statist.*, vol. 41, pp. 337–348, 1992.
- [15] A. Curvers and P. Van der Werff, "OWEZ wind farm efficiency," Tech. Rep. ECN-E-08-092, 2008. [Online]. Available: <ftp://ftp.ecn.nl/pub/www/library/report/2008/e08092.pdf>
- [16] A. Raftery and S. Lewis, "One long run with diagnostics: Implementation strategies for Markov chain Monte Carlo," *Statist. Sci.*, vol. 7, no. 4, pp. 493–497, 1992.
- [17] H. Yang, K. Xie, H.-M. Tai, and Y. Chai, "Wind farm layout optimization and its application to power system reliability analysis," *IEEE Trans. Power Syst.*, vol. 31, no. 3, pp. 2135–2143, May 2016.
- [18] A. Pourhabib, J. Z. Huang, and Y. Ding, "Short-term wind speed forecast using measurements from multiple turbines in a wind farm," *Technometrics*, vol. 58, no. 1, pp. 138–147, 2016.
- [19] E. Byon, Y. Choe, and N. Yampikulsakul, "Adaptive modeling and prediction in time-variant processes with application to wind power systems," *IEEE Trans. Autom. Sci. Eng.*, vol. 13, no. 2, pp. 997–1007, Apr. 2016.
- [20] P. M. O. Gebraad *et al.*, "Wind plant power optimization through yaw control using a parametric model for wake effects—a CFD simulation study," *Wind Energy*, vol. 19, no. 1, pp. 95–114, 2016.
- [21] P. Z. G. Qian and C. F. J. Wu, "Bayesian hierarchical modeling for integrating low-accuracy and high-accuracy experiments," *Technometrics*, vol. 50, no. 2, pp. 192–204, 2008.



**Eunshin Byon** (S'09–M14) received the Ph.D. degree in the Department Industrial and Systems Engineering, Texas A&M University, College Station, TX, USA, in 2010. She is currently an Associate Professor with the Department of Industrial and Operations Engineering, University of Michigan, Ann Arbor, MI, USA. Her research interests include data analytics, quality and reliability engineering, condition monitoring, operations and maintenance optimization, and uncertainty quantification. She is a member of IIE, INFORMS, and ASQ.



**Shuai Huang** (M'12) received the B.S. degree in statistics from the University of Science and Technology of China, Hefei, China, in 2007, and the Ph.D. degree in industrial engineering from Arizona State University, Tempe, AZ, USA, in 2012. He is currently an Assistant Professor with the Department of Industrial and Systems Engineering, University of Washington, Seattle, WA, USA. His research interests include statistical learning and data mining with applications in healthcare and manufacturing. He is a member of INFORMS, IIE, and ASQ.



**Mingdi You** (S'16) received the B.S. degree in mathematics from Southeast University, Nanjing, China, and the M.S. degree in industrial and operations engineering from the University of Michigan, Ann Arbor, MI, USA. He is currently working toward the Ph.D. degree in the Department of Industrial & Operations Engineering, University of Michigan. His research interest includes applied statistics and spatial data analytics and reliability engineering with applications on wind energy. He is a student member of IIE and INFOMRS.



**Bingjie Liu** received the B.S. degree in industrial and systems engineering from the University of Wisconsin, Madison, WI, USA, in 2015. She is currently working toward the Ph.D. degree in the Department of Industrial and Operations Engineering, University of Michigan, Ann Arbor, MI, USA. Her research interests include computer model calibration, data analytics, and quality and reliability engineering.



**Jionghua (Judy) Jin** (M'06) received the Ph.D. degree in 1999 from the University of Michigan, Ann Arbor, MI, USA, where she is currently a Professor with the Department of Industrial and Operations Engineering. Her research focuses on data fusion in quality and reliability engineering for improving complex systems operations. Her research emphasizes the integration of applied statistics, signal processing, reliability, system modeling, and decision-making theory. Her research has been broadly applied to various applications including both manufacturing and service industries, such as metal forming, automotive manufacturing, solar battery and wind power systems, medical clinical decision-making, unmanned ground vehicles, and transportation. She has received a number of awards including the NSF CAREER and PECASE Awards, and ten Best Paper Awards. She is a Fellow of ASME and IIE, a senior member of ASQ and ISI, and a member of INFORMS and SME.